

## Fabrication of *in situ* ultrathin anodic aluminum oxide layers for nanostructuring on silicon substrate

Bo Yan<sup>a)</sup> and Hoa T. M. Pham

Laboratory of Electronic Components, Technology and Materials (ECTM), Delft Institute of Microelectronics and Submicron Technology (DIMES), Delft University of Technology, Feldmannweg 17, 2600 GB Delft, the Netherlands

Yue Ma and Yan Zhuang

Laboratory of High Frequency Technology (HiTech), Delft Institute of Microelectronics and Submicron Technology (DIMES), Delft University of Technology, Mekelweg 4, 2628 CD Delft, the Netherlands

Pasqualina M. Sarro

Laboratory of Electronic Components, Technology and Materials (ECTM), Delft Institute of Microelectronics and Submicron Technology (DIMES), Delft University of Technology, Feldmannweg 17, 2600 GB Delft, the Netherlands

(Received 17 May 2007; accepted 9 July 2007; published online 2 August 2007)

The authors demonstrate a method for the fabrication of *in situ* ultrathin porous anodic aluminum oxide layers (aspect ratio < 2:1) on Si, which can be directly used as templates for nanodot preparation and for pattern transfer. The regular shape of the aluminum oxide pores is maintained even when the thickness of the aluminum oxide template is reduced to 50 nm. By using these *in situ* ultrathin templates as lift-off masks, the authors successfully prepared a  $\text{Ba}_x\text{Sr}_{1-x}\text{TiO}_3$  nanodot array on Si surface. Furthermore, these nanotemplates are employed as lithographic masks to transfer the nanopattern into the silicon substrate. © 2007 American Institute of Physics.

[DOI: 10.1063/1.2767768]

Recently, porous anodic aluminum oxide (AAO) templates have received quite some attention for application in nanowire and nanotube synthesis, due to the ideal pore diameters and high aspect ratio of their channels.<sup>1-3</sup> Generally, AAO templates exhibit columnar pore structure, vertical to the substrate and parallel to each other with pore diameters from several tens to several hundreds nanometers and with an aspect ratio between 10 and 1000 or more.<sup>4-9</sup> Thus, by filling the pores of the AAO templates, arrays of well aligned nanowires and nanotubes with uniform diameter and length can be obtained by electroplating or other growth methods.

However, the use of AAO templates for nanodot deposition and nanopattern transfer masks, an interesting approach for the fabrication of nanostructures without the need of costly nanolithography, is often impaired by this high aspect ratio. In fact, for high aspect ratio templates, the filling of the pores during deposition is poorer and dry etching for pattern transfer is more difficult. Furthermore, the channel sidewalls tend to be less smooth, which negatively affect the above-mentioned nanostructuring processes.<sup>8</sup> Therefore, it is very important to reduce the aspect ratio of the templates when we employ them for nanostructuring Si substrates. A few methods have been developed to prepare ordered ultrathin AAO mask.<sup>7,8</sup> In these methods, the bulk Al is chosen as starting material, and then after anodization AAO templates are released from the Al substrate and mounted on the surface of Si or  $\text{SiO}_2$  substrates to act as deposition masks. However, AAO is like a brittle ceramic film. Great attention needs to be paid in the manipulation. Moreover, these methods are not very compatible with the conventional integrated circuit (IC) processes, which restrict their application in Si based structures. Thus it would be a great benefit to realize *in situ* ultrathin AAO mask layers directly on a Si substrate.

In this letter, we report on a simple method to fabricate *in situ* ultrathin AAO templates (aspect ratio < 2:1) on Si substrate. As schematically shown in Figs. 1(a) and 1(b), after the ordered thicker AAO template on Si substrate is obtained by anodization, an additional step is introduced which makes use of the capillary effect (antiwetting) to only etch the surface of AAO template and not the sidewalls of

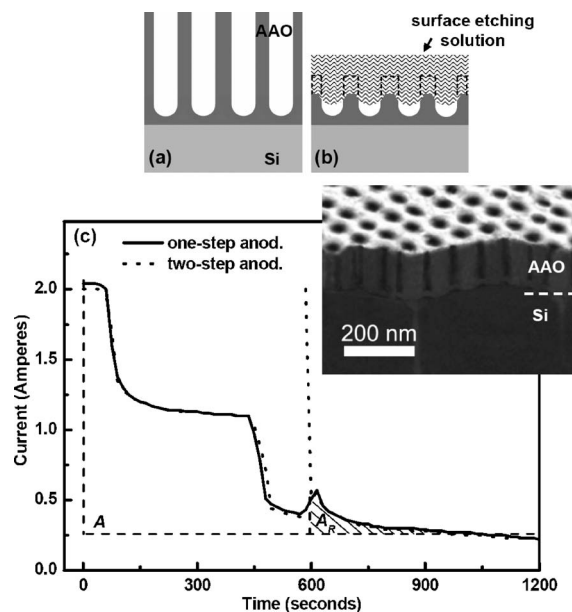


FIG. 1. Schematic drawing of (a) the template after the anodization step and (b) the capillary effect to reduce the final thickness. (c) Current-time ( $I-t$ ) curve for anodization of sputtered Al/1%Si layers in oxalic acid at 40 V. The solid curve corresponds to the one-step anodization. The dotted curve represents the two-step anodization process with a first anodization time of 600 s. The letter A represents the whole area under the solid curve; the  $A_R$  corresponds to the area under the second part of the dotted curve. The SEM image shows the cross section of the sample just before the thinning step.

<sup>a)</sup>Electronic mail: b.yan@tudelft.nl

the pores. The final thickness of the templates is decreased to about 50 nm while the size and shape of the entire template are not altered.

To demonstrate the potential of this process, these ultrathin AAO templates are used as molds to prepare  $\text{Ba}_x\text{Sr}_{1-x}\text{TiO}_3$  (BST) nanodot array on Si surface and to transfer the AAO template pattern onto the Si surface. In this study, the morphology and microstructure of the templates, as well as the nanodot arrays and transferred pattern are examined by scanning electron microscopy (SEM) (Fei XL30 SFEG) and atomic force microscopy (AFM) (Ntegra PNL) analyses.

As anodization substrates of 4 in. *p*-type silicon wafers with a rf-sputtered 4  $\mu\text{m}$  thick Al/1%Si layer are used. The anodization of the Al layer is performed in 0.3M oxalic acid solution at room temperature, using an anodization voltage of 40 V. The additional thinning step gives much better results if the initial AAO template thickness is not more than 200 nm. Therefore, the current-time (*I-t*) variation is monitored and recorded to determine the AAO template thickness after the anodization process. The typical *I-t* curve of the experiment is shown in Fig. 1(c). The solid curve and the dotted curve correspond to the one-step and the two-step anodization processes, respectively. The quantity of electricity (*Q*) exchanged during the anodization is proportional to the Al consumed.<sup>9-11</sup> Therefore, we can roughly calculate the amount of consumed Al and transformed in  $\text{Al}_2\text{O}_3$  in different anodization steps. The ratio between the remaining and the original Al thickness is equal to  $A_R/A$ , where  $A_R$  is the integral area under the second part of the dotted curve (shaded region) and *A* is the whole integral area under the one-step curve (the solid curve). For the two-step anodization sample  $A_R/A$  is  $4.8 \pm 0.5\%$  and the original thickness of the Al layer before anodization is 4  $\mu\text{m}$ . This means that the remaining Al thickness of the template can be estimated as  $192 \pm 20$  nm. After the anodic oxidation the resulting porous aluminum oxide layer will be 1.2 times that of the initial Al layer.<sup>12</sup> Therefore, the final thickness of the template after anodization can be expected to be  $230 \pm 24$  nm. The inserted cross-sectional SEM image of the two-step anodization sample shown in Fig. 1(c) indicates that the thickness of AAO template is indeed  $\sim 200$  nm. This value is very close to the predicted thickness, considering that the unstable period at the beginning of the anodization and the local concentration fluctuation may cause an etching rate variation.

In fact, some amount of Al needs to be consumed during the initial unstable period of anodization to enter the ordered pore formation period. Therefore, an ordered ultrathin AAO template directly prepared by anodization is difficult and the employment of the additional thinning step is necessary. As schematically shown in Figs. 1(a) and 1(b), the thickness of template is reduced by making use of the capillary effect to prevent the acid solution from entering the channels of the AAO template. In fact, this one-end closed pore structure is like a potential capillary tube, which can prevent aqueous acid from entering the holes effectively. However, the pore surface of the AAO template, being dried in air after the anodization process presents Al-O bonds and is rather hydrophilic. Therefore, the pore surface of the AAO template is made hydrophobic by octatrachlorosilane.<sup>13</sup> After the silanization process, the AAO template surface is etched in 3 wt %  $\text{H}_3\text{PO}_4$  acid at 30 °C. Figure 2(a) shows the SEM images of a sample after the additional thinning step. From a

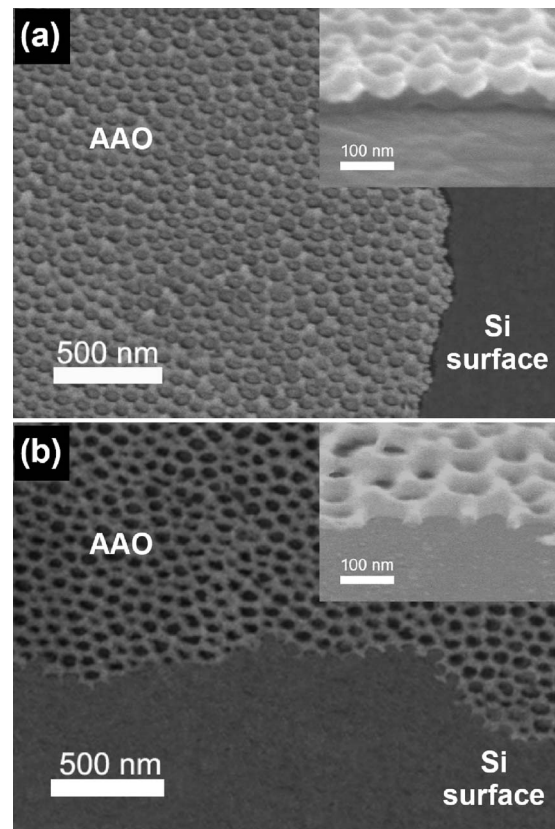


FIG. 2. SEM images of an *in situ* ultrathin AAO template (a) before and (b) after the etching (by RIE) of the barrier layer. The inserted images show the cross-sectional profile of the two corresponding samples.

statistical analysis of these samples, the density of the pore is about  $1.22 \times 10^{10} \text{ cm}^{-2}$ , while more than 70% of the pores have a diameter between 50 and 70 nm. The details of the structure are shown in the inserted cross-sectional image. This picture clearly shows that even if the thickness of the template reduces to about 50 nm, the shape of the holes is well preserved, especially the continuous and dense barrier layer of the channels is still intact. This means that even in this stage, the capillary effect still prevents the acid solution from entering the holes to affect the barrier layer.

To obtain direct physical and electrical contact between the channel and the substrate as necessary for the nanodot deposition and pattern transfer purposes, the exposed barrier layer is etched away by a very short (30 s) reactive ion etching (RIE) in  $\text{BCl}_3$ . As shown in Fig. 2(b), the barrier layer of the AAO template has been opened while the whole template is not damaged. This is clearly an advantage with respect to the continuous anodization approach previously reported,<sup>14,15</sup> in which after the barrier layer reaches the Si surface, anodic oxidation of Si will happen. This comes with the generation of hydrogen ions, leading to the excessive dissolution of aluminum oxide between the pore base and the Si surface, thus forming voids directly beneath the barrier layer.

BST nanodots and pattern transfer to Si surface are performed to illustrate the potential of these *in situ* ultrathin (50–100 nm thick, with pore diameter of about 70 nm) AAO templates as nanostructuring tool. Spin coating of BST sol-gel solution is employed as deposition method. The spin speed is 2000 rpm. After spin coating, the film is annealed at 750 °C to allow the sol-gel precursors to crystallize. Then, the ultrathin AAO templates are lifted off in  $\text{H}_3\text{PO}_4$

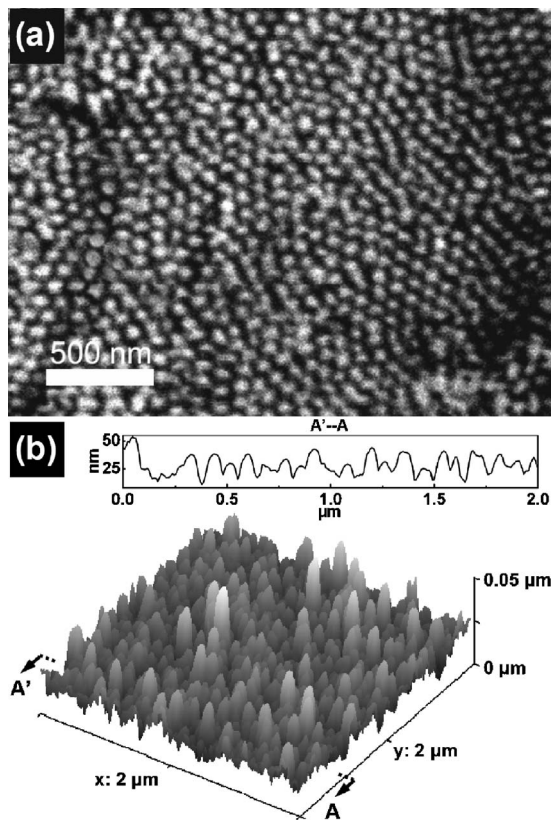


FIG. 3. BST nanodot array on Si surface: (a) SEM image after lift-off of the AAO mask layer and (b) three-dimensional AFM image. A representative height profile along the A'-A line in the image is included. The height of the BST nanodots is below 50 nm.

(3 wt %) acid solution at 30 °C, leaving the array of  $\text{Ba}_x\text{Sr}_{1-x}\text{TiO}_3$  ( $0 < x < 1$ ) nanodots on the Si surface. From the SEM and AFM observations in Fig. 3, the density is  $\sim 1.22 \times 10^{10} \text{ cm}^{-2}$  and the diameter of these ferroelectric nanodots is  $\sim 70 \text{ nm}$ . It is clear that the shape and density of BST nanodots inherited the AAO template shape. A representative height profile along the dotted line A'-A in the image is presented.

In addition, the AAO nanotemplate is used as a masking layer to nanopattern the silicon. The exposed silicon surface is etched by RIE with  $\text{Cl}_2$  and  $\text{BCl}_3$  as etching gases. The etch rate of bulk Si in the conditions used is 200 nm/min. The SEM images in Fig. 4 reveal the silicon surface after the pattern transfer and after the removal of the AAO masking layer. It can be clearly seen that the density of the nanohole array ( $1.19 \times 10^{10} \text{ cm}^{-2}$ ) and the shape of the holes are maintained after dry etching. The diameter of the holes is 30–50 nm, which is slightly smaller than that of the pores of the AAO template, due to the redeposition effect.<sup>16</sup> For the 1.5 min etch used, a depth of nanoholes of about 80 nm is obtained. The etch rate of Si when using the AAO mask is much lower than that of bulk Si in the same etching conditions. This is essentially due to the small openings in the AAO mask layer that cause a lower plasma density hitting the Si surface and thus decreasing the etching efficiency of the RIE process.

In conclusion, *in situ* ultrathin AAO layers (aspect ratio  $< 2:1$ ) on Si surface are successfully fabricated by taking advantage of the capillary effect. The investigation on the mask morphology demonstrates that the thickness of ultra-

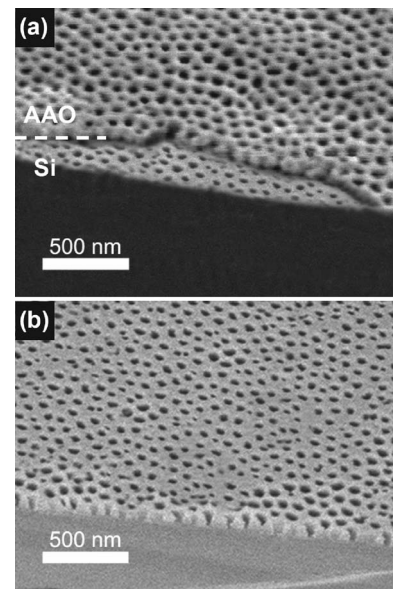


FIG. 4. SEM images of the Si surface after the AAO template pattern transfer: (a) AAO template not removed and (b) after removal of the template. The diameter of the nanoholes varies between 30 and 50 nm and the depth of the holes is about 80 nm.

thin AAO masks can be as small as 50 nm, and the shape of the template is well maintained with no etching solution entering the channels to damage the whole template. These ultrathin AAO templates are used as molds to form BST nanodot arrays or as masks to transfer the AAO template pattern to the Si substrate. From the SEM observation, the size parameters of nanodot array on Si surface and nanoholes in Si are consistent with those of the AAO templates. The present work proposes a promising fabrication method to prepare nanostructures in and on silicon without the use of costly and complex nanolithography.

This work was partly supported by FOM (Project No. FOM-D-11). The authors would like to thank the DIMES IC process group for the support during sample preparation.

<sup>1</sup>H. Masuda and P. Fukuda, *Science* **268**, 1466 (1995).

<sup>2</sup>A. P. Li, F. Müller, A. Birner, K. Nielsch, and U. Gösele, *Adv. Mater. (Weinheim, Ger.)* **11**, 483 (1999).

<sup>3</sup>J. Li, C. Papadopoulos, J. M. Xu, and M. Moskovits, *Appl. Phys. Lett.* **75**, 367 (1999).

<sup>4</sup>D. Crouse, Y. H. Lo, A. E. Miller, and M. Crouse, *Appl. Phys. Lett.* **76**, 49 (2000).

<sup>5</sup>P. L. Chen, C. T. Kuo, T. G. Tsai, B. W. Wu, C. C. Hsu, and F. M. Pana, *Appl. Phys. Lett.* **82**, 2796 (2003).

<sup>6</sup>H. Asoh, K. Sasaki, and S. Ono, *Electrochem. Commun.* **7**, 953 (2005).

<sup>7</sup>H. Masuda, H. Yamada, M. Satoh, H. Asoh, M. Nakao, and T. Tamamura, *Appl. Phys. Lett.* **71**, 2770 (1997).

<sup>8</sup>Y. Lei and W. K. Chim, *Chem. Mater.* **17**, 580 (2005).

<sup>9</sup>L. Pu, Y. Shi, J. M. Zhu, X. M. Bao, R. Zhang, and Y. D. Zheng, *Chem. Commun. (Cambridge)* **8**, 924 (2004).

<sup>10</sup>G. E. Thompson, Y. Xu, P. Skeldon, K. Shimizu, S. H. Han, and G. C. Wood, *Philos. Mag. A* **55**, 651 (1987).

<sup>11</sup>F. Li, L. Zhang, and R. M. Metzger, *Chem. Mater.* **10**, 2470 (1998).

<sup>12</sup>K. Nielsch, J. Choi, K. Schwirn, R. B. Wehrspohn, and U. Gösele, *Nano Lett.* **2**, 677 (2002).

<sup>13</sup>J. J. Qiao, X. H. Zhang, X. M. Meng, S. M. Zhou, S. K. Wu, and S. T. Lee, *Nanotechnology* **16**, 433 (2005).

<sup>14</sup>M. T. Wu, I. C. Leu, and M. H. Hon, *J. Mater. Res.* **19**, 888 (2004).

<sup>15</sup>S. Z. Chu, K. Wada, S. Inoue, and S. Todoroki, *J. Electrochem. Soc.* **149**, B321 (2002).

<sup>16</sup>S. Shingubara, O. Okino, Y. Murakami, H. Sakaue, and T. Takahagi, *J. Vac. Sci. Technol. B* **19**, 1901 (2001).